RSC Advances

PAPER

Cite this: *RSC Adv.*, 2023, **13**, 1312

An efficient calcium-based sorbent for flue gas dry-desulfurization: promotion roles of nitrogen oxide and oxygen†

Kai-Qi Wang,[a] Xian-Ming Gao,[b] Bo Lin,*[a] Dong-Xu Hua,[b] Yong Yan,[a] Hong-Yan Zhao[b] and Wen-De Xiao *[a]

The development of sorbents for flue gas desulfurization in a dry mode is essential to control emission of sulfur dioxide. Based on the novel concept of "treating waste with waste", a low-cost and highly activated calcium-based sorbent (ACS) was prepared using coal fly ash, CaO and waste gypsum as the raw materials *via* the one-step incipient wetness impregnation method. Based on characterization using scanning electron microscopy and nitrogen adsorption–desorption, the ACS possessed a fibrous and netted structure with high porosity, which improved SO_2 adsorption greatly. The SO_2 adsorption capacity of ACS with coal fly ash/CaO/$CaSO_4$ = 1/2/1 was high, up to 44.26 mg g^{-1}, with 100% removal efficiency at 150 °C. In the absence of O_2, SO_2 was rapidly adsorbed on the sorbent to form $CaSO_3$ according to *in situ* DRIFTS analysis, while when O_2 was present in the flue gas, SO_2/SO_3^{2-} tended to be oxidized into SO_4^{2-} species. Moreover, the presence of NO can further enhance the SO_2 adsorption capacity of the ACS due to the formation of adsorbed NO_2 or nitrate species with strong oxidizing properties. Therefore, the ACS can be considered as a sustainable sorbent with the advantage of employing fly ash for the removal of sulfur dioxide.

Received 13th September 2022
Accepted 14th December 2022

DOI: 10.1039/d2ra05769g

rsc.li/rsc-advances

1. Introduction

Industry activity related haze problems have drawn more and more attention worldwide. Coke oven plants, as the dominant stationary pollution source, discharge massive amounts of air pollutants, mainly including SO_2 and NO_x.[1–3] Currently, flue gas desulfurization (FGD) processes are widely applied for the elimination of SO_2 emissions. According to the type of desulfurizer and the state of the resultant outflow, FGD methods can be classified into wet flue gas desulfurization, semi-dry flue gas desulfurization and dry flue gas desulfurization. In the wet-scrubbing technique,[4] the overall reaction (1) occurs as follows:

$$SO_2(g) + CaCO_3(s) + 0.5O_2(g) + 2H_2O(l) \rightarrow CaSO_4 \cdot 2H_2O(s) + CO_2(g) \quad (1)$$

Despite its high efficiency, costly equipment investment requirements and easy scale formation causing pipe blockages have restrained the application of the wet-scrubbing technique. Besides, the desulfurization unit is usually installed in front of a denitrification unit in coke oven industrial practice.[5] Generally, the operation temperature of wet FGD is around 45–60 °C,[6] which is too low for low-temperature selective catalytic reduction (LT-SCR) flue gas denitrification technology.[7] Consequently, more additional energy has to be consumed to heat the feed gas for SCR. Considering the temperature mismatch and energy consumption involved in the wet FGD process, dry and semi-dry FGD techniques are alternative effective approaches, particularly under low-concentration SO_2 operating conditions. Compared with the wet-scrubbing method, dry and semi-dry FGD techniques cost less since less energy is required and no waste water is produced.[4] Furthermore, with the development of circulating fluidized bed flue gas desulfurization technology, dry and semi-dry flue gas desulfurization technologies have been paid close attention in China.

Nevertheless, for dry and semi-dry FGD technologies, there is still enormous difficulties and challenges going from advanced process to practical industrial application. The primary subsistent problem is the unsatisfactory desulfurization efficiency. Nowadays, the main desulfurizers used in dry and semi-dry FGD technologies include activated coke desulfurizers,[8–10] calcium desulfurizers[11–14] and supported desulfurizers.[15] Among the above desulfurizers, the calcium desulfurizer is the most common commercial sorbent in industrial application. In order to synthesize calcium-based sorbents with higher SO_2 adsorption activity, most siliceous materials reported in previous research like coal fly ash,[16–18] diatomite,[19] oil palm ash[20] and rice husk ash (RHA)[21,22] can be

[a]School of Chemistry and Chemical Engineering, Shanghai Jiao Tong University, Shanghai 200240, P.R, China. E-mail: wdxiao@sjtu.edu.cn
[b]Henan Shenma Nylon Chemical Company, Ltd, Henan 467013, P.R. China

† Electronic supplementary information (ESI) available. See DOI: https://doi.org/10.1039/d2ra05769g

activated with calcium oxide (CaO) or calcium hydroxide ($Ca(OH)_2$). The siliceous materials are primarily composed of silica (SiO_2) and alumina (Al_2O_3), which react with $Ca(OH)_2$ to generate calcium aluminate silicate hydrate compounds ($(CaO)_x(Al_2O_3)_y(SiO_2)_z(H_2O)_w$). This reaction is the well-known "pozzolanic reaction".[23] Since the reaction products are generally amorphous with comparably high specific surface areas, the adsorption capacity of the sorbent for sulfur dioxide (SO_2) is remarkably improved.[13,24] Among the above-mentioned siliceous materials, fly ash as a typical industrial waste product has attracted much interest due to the fact that it contains abundant metal elements such as calcium, iron, aluminum, magnesium and others, which can enhance SO_2 adsorption in flue gases. Indeed, fly ash is an excellent precursor to prepare low-cost and high-efficiency sorbents for treatment of environment pollutants.[18] For instance, it was reported that the addition of fly ash solution to $Ca(OH)_2$ could prepare an active material for SO_2 removal.[25] Additionally, the effect of the fly ash/$Ca(OH)_2$ ratio and slurrying temperature on desulfurization efficiency was investigated. The increase of temperature could significantly enhance the utilization rate of calcium.[26] Moreover, it was found that fly ash/$Ca(OH)_2$ sorbents prepared in a Parr pressure reactor contributed to the removal of SO_2.[27] These results indicated that a sorbent prepared by mixing fly ash with $Ca(OH)_2$ could show enhanced removal performance of SO_2. However, an increase of $Ca(OH)_2$ cannot increase the release rate of silica and alumina from fly ash, constraining the further improvement of desulfurization performance over fly ash/$Ca(OH)_2$ sorbents. Hence, $Ca(OH)_2$ was substituted with CaO to prepare sorbents since the exothermic reaction of CaO with water dramatically promotes the pozzolanic reaction. Furthermore, it was confirmed that the waste product gypsum ($CaSO_4$) is a chemical activator incorporated in fly ash that contributes to the formation of mesoporous structure.[28] Additionally, the presence of $CaSO_4$ could improve the leaching rate of silica and alumina from the coal fly ash.[17] Consequently, we designed a novel calcium-based sorbent consisting of coal fly ash, CaO and gypsum. Herein, a one-step incipient wetness impregnation method was applied to prepare a highly activated calcium-based sorbent from coal fly ash, CaO and gypsum. A series of sorbents with similar specific surface areas were prepared to study the effect of different raw material ratios on SO_2 removal performance. By using characterization techniques such as X-ray diffraction (XRD), scanning electron microscopy (SEM) and nitrogen adsorption and desorption analysis, the structure and properties of the novel calcium-based sorbent were illuminated. Notably, the mechanism of SO_2 adsorption on this desulfurizer along with the effect of O_2 and NO on the desulfurization process was first investigated integrally *via in situ* diffuse reflectance infrared Fourier transform spectroscopy (DRIFTS) experiments. The research results contributed to the optimization of process conditions and the development of an efficient calcium-based sorbent with an optimal ratio, which has great significance for achieving the goal of ultra-low emission of coal-fired power plant flue gas.

2. Experimental

2.1 Sorbent preparation

The coal fly ash, which was provided by a coal-fired power plant of Henan Yulian Energy Group, China, was mixed with CaO and $CaSO_4$ (Sinopharm) *via* a one-step incipient wetness impregnation method to synthesize the highly activated calcium-based sorbent at a low temperature (90 °C) in a hydration reactor. Cui *et al.*[29] used the preparation technology of adsorbents to study the desulfurization mechanism of adsorbents prepared using high ratio circulating fly ash and lime. Based on this, appropriate amounts of coal fly ash, CaO and $CaSO_4$ were dissolved in distilled water under vigorous stirring at 90 °C for 6 h and dried at 120 °C overnight. The obtained sorbents were denoted as ACS-1, ACS-2, ACS-3, ACS-4 and ACS-5 (Table S1†), respectively, with different ratios of fly ash/CaO/$CaSO_4$. Before each test, the sample was crushed into fine particles with an approximately 40–60 mesh, small enough to eliminate the effects of inner diffusion resistance.

2.2 Physical and chemical properties analysis

The specific surface area, pore volume and pore size of the sorbents were determined by nitrogen adsorption at 77 K using a surface area analyzer (Quantachrome ASIQA3200-3, America). The surface area was calculated from the nitrogen adsorption–desorption isotherms, according to the Brunauer–Emmett–Teller (BET) equation. The pore size distribution was determined by the Barrett–Joyner–Halenda (BJH) method. The samples were degassed under vacuum at 150 °C for 12 h prior to measurement of the surface area and pore size distribution. The crystal structure of the samples was characterized by X-ray diffraction (XRD) using an XRD spectrometer (D8 Advance, Bruker, Germany) with Cu Kα ($\lambda = 1.5056$ Å) radiation, operated at 40 kV and 200 mA. In particular, the samples loaded on a sample holder at a depth of about 1 mm were tested over a 2θ range of 5–90° at a speed of 6° min^{-1}. Thermogravimetric analysis (TGA) experiments were performed in a Thermogravimetric Analyser Q500 from TA Instruments to study the thermal decomposition behavior of the as-synthesized sorbents. The surface morphology and structure of the as-synthesized sorbents were imaged by scanning electron microscopy (SEM, Sirion 200). The sample treatment process was as follows: first, conductive tape was glued on the sample table, and then the powder sample was evenly sprinkled on the conductive glue. Then, the sample that did not stick was blown off with an ear washing ball. Finally, the samples were plated with platinum and then observed using the scanning electron microscope. The acceleration voltage was 10 kV. Fourier transform infrared (FTIR) spectra were recorded using a FT-IR spectrometer (PerkinElmer Frontier, America) at 4 cm^{-1} resolution with an accumulation of 32 scans by KBr optics and a TGS detector. The samples mixed with KBr powder were put into an agate milk bowl and ground evenly, and then loaded into a pressing mold to prepare the KBr sample. The whole operation was carried out under an infrared lamp to prevent moisture absorption. *In situ* DRIFTS spectra were recorded on a PE Frontier IR spectrometer

equipped with a liquid-nitrogen-cooled MCT detector using a temperature-controlled DRIFTS chamber with ZnSe windows. Prior to each experiment, the sample was pretreated at 150 °C for 1 h in flowing N_2 (50 mL min^{-1}) to clean the sorbent surface for a background spectrum to be automatically generated. The reaction conditions were controlled as follows: 1000 mg m^{-3} SO_2, and/or 750 mg m^{-3} NO and/or 8% O_2 and pure N_2 balance gas, and 200 mL min^{-1} total flow rate. All spectra were recorded by accumulating 32 scans with a resolution of 4 cm^{-1}. For each experiment under different test conditions, a fresh sorbent was used.

2.3 Desulfurization performance tests

An experimental instrument was established to evaluate the desulfurization performance of the highly activated calcium-based sorbent under atmospheric pressure in the dry FGD process, as shown in Fig. 1. The fixed-bed reactor was composed of a U-shaped stainless steel (S31603) tube with an internal diameter of 6 mm and a total length of 1 m, immersed in a salt bath for temperature control. The sorbent (2 g) was packed in the center of the reactor supported by glass wool. For the avoidance of sorbent clumps causing flue gas short circuit, the sorbent bed was packed with a sorbent/silica sand ratio of 1/5 to obtain an isothermal bed. The flow rate of the feed gas (N_2, O_2, NO and SO_2) was controlled by thermal mass flow controllers. The different gas was blended and preheated in a gas mixer to form the simulated flue gas. After stable working conditions were obtained, the bypass of the reactor was closed and the U-shaped tube desulfurization reactor was available for desulfurization experiments. The gas passed through the reactor at a total flow rate of 600 mL min^{-1}. The content of feed gas and products was continuously monitored by a flue gas analyzer (Vario Plus; MRU, Germany). Besides, the instrument error was ±3 ppm. For each condition, the sorbent was purged with nitrogen for 1 h. The desulfurization activity was measured by SO_2 conversion expressed by the following equation:[30]

$$SO_2\ \text{conversion} = \frac{SO_{2\,in} - SO_{2\,out}}{SO_{2\,in}} \times 100\% \quad (2)$$

where $SO_{2\ in}$ represents the concentration of SO_2 at the inlet and $SO_{2\ out}$ represents the concentration of SO_2 at the outlet.

Finally, the adsorption capacity of the sorbent for SO_2 was calculated by using a SO_2 adsorption penetration curve, whereby the following equation was adopted:[31]

$$q = \frac{Q \times C_0 \int_0^t [1 - f(t)]\mathrm{d}t}{m} \quad (3)$$

where q is the dynamic adsorption capacity (mg SO_2 (g sorbent)$^{-1}$), Q is the total gas flow rate (m^3 min^{-1}), C_0 is the initial concentration (mg m^{-3}), $f(t)$ is SO_2 conversion (%), t is the adsorption time (min), and m is the amount of sorbent (g).

3. Results and discussion

3.1 Desulfurization performance

The desulfurization performance of all the as-synthesized sorbents and raw materials was tested in an isothermal fixed bed reactor as mentioned above. The activity tests were conducted by feeding 1000 mg m^{-3} SO_2, 750 mg m^{-3} NO, 8% O_2, and N_2 as the balance gas at 150 °C with a gas hour space velocity (GHSV) of 12 000 h^{-1}. As Fig. 2(a) displays, $CaSO_4$ and fly ash could hardly capture SO_2, while CaO only maintained 100% SO_2 removal ratio for 7 min, followed by rapid inactivation. Notably, the mixture of fly ash/CaO/$CaSO_4$ showed distinctly improved desulfurization performance. Among the series of sorbents with different ratios of fly ash/CaO/$CaSO_4$, ACS-4 showed the most outstanding SO_2 elimination efficiency maintaining 100% SO_2 removal for 43 min. Moreover, the deactivation rate of ACS-4 was significantly decreased compared with the other sorbents. At the time on stream of 120 min, SO_2 removal dropped to around 25%. Besides, the dynamic adsorption amount of SO_2 was calculated by using eqn (3), as shown in Fig. 2(b). Indeed, the SO_2 adsorption capacities of the ACS with different fly ash/CaO/$CaSO_4$ ratios followed the order of ACS-4 (44.26 mg g^{-1}) > ACS-3 (33.85 mg g^{-1}) > ACS-5 (28.21 mg g^{-1}) > ACS-2 (26.28 mg g^{-1}) > ACS-1 (12.42 mg g^{-1}). In summary, the combination of fly ash/CaO/$CaSO_4$ shows superior SO_2 adsorption capacity compared with each single component and the optimal ratio of fly ash/CaO/$CaSO_4$ is 1 : 2 : 1. Additionally, the SO_2 adsorption capacity of various previously reported Ca-based sorbents is listed in Table 1. The SO_2 adsorption amount of the sorbent prepared in this work (ACS-4)

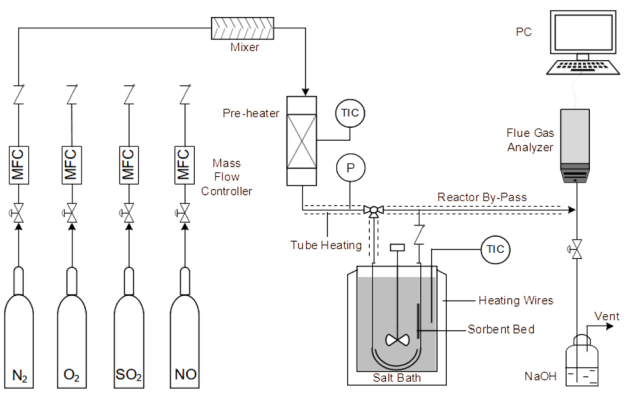

Fig. 1 Experimental fixed-bed set-up for desulfurization.

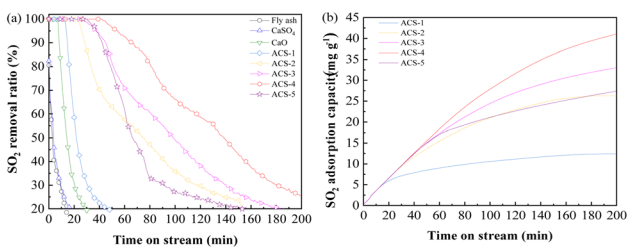

Fig. 2 (a) Desulfurization activity of the different as-synthesized sorbents and raw single components (the reactant feed contains 1000 mg m^{-3} SO_2, 750 mg m^{-3} NO, and 8% O_2 balanced with N_2 at a GHSV of 12 000 h^{-1} and a temperature of 150 °C). (b) The SO_2 adsorption capacity of the sorbents: SO_2 accumulated adsorption capacity as a function of time.

Table 1 Comparison of adsorption amount between ACS-4 and various Ca-based sorbents reported previously

Sorbent	Adsorption amount (mg g^{-1})	S_{BET}, (m^2 g^{-1})	Ref.
RHA/CaO/$CaSO_4$	17.14	65.3	7
RHA/CaO/NaOH	19.73	28.7	24
CaL_2	24.8	—	32
Calcium silicate	38.2	174	31
50CaO/CFoam	46.85	183.2	33
ACS-4	44.26	31.43	This work

surpasses that of a majority of Ca-based sorbents except for the 50CaO/C Foam material. Nevertheless, the differences in SO_2 adsorption capacity between ACS-4 and 50CaO/CFoam are insignificant. By contrast, the sorbent prepared in this work (ACS-4) presents considerable potential in future practical application due to its outstanding desulfurization performance and low cost.

3.2 Sorbent characterization

The pore structure parameters of the three raw materials and the as-synthesized sorbents are listed in Table 2. The specific surface area along with pore volume and average pore size of the active raw materials were extremely small, leading to poor desulfurization efficiency. Particularly, the pore volume of fly ash was only 0.003 cm^3 g^{-1}, indicating that fly ash has little pore structure. According to previous literature,[34] the main chemical constituents of original fly ash are compounds mainly composed of amorphous SiO_2 and Al_2O_3, which can be dissolved in alkaline solutions and then react with Ca^{2+}. The reaction between fly ash and calcium hydroxide is known as a pozzolanic reaction and yields calcium aluminate silicate hydrate compounds that are fibrous gels that have improved surface areas, pore volumes and hierarchical networks. In contrast, the specific surface area, pore volume and the average pore size of the prepared ACS was markedly increased in comparison to the original materials, which suggested that the hydration reaction process had a positive influence on the surface area of the sorbent. It was speculated that the heat released during the hydration reaction greatly swelled the inner pores, causing the increase of specific surface area. Additionally, the nitrogen adsorption–desorption isotherms and pore diameter distributions of the ACS are illustrated in Fig. S1.† All of the sorbents revealed typical Langmuir IV isotherm curves with a type H3 hysteresis loop, indicating the existence of slit-like mesopores in aggregates.[18,19] The pore size distributions of all the ACSs further verified the existence of mesopores (2–50 nm). Among them, the pore diameter distribution of ACS-4 was most concentrated and homogeneous (around 30 nm), which may provide abundant adsorption active sites for desulfurization reaction. In conclusion, the combination reaction of the three raw components increased the specific surface area of the ACS, which facilitated the desulfurization reaction compared with the single components. ACS-4 with the biggest specific surface area, pore volume and average pore size presented the most outstanding desulfurization performance.

Table 2 Pore structure parameters of the samples

Samples	S_{BET}, (m^2 g^{-1})	V_p, (cm^3 g^{-1})	d_p, (nm)
Fly ash	1.45	0.003	6.89
CaO	4.21	0.011	9.94
$CaSO_4$	1.65	0.045	10.83
ACS-1	28.49	0.116	16.34
ACS-2	28.59	0.158	22.08
ACS-3	29.29	0.139	18.99
ACS-4	31.43	0.176	22.34
ACS-5	21.24	0.111	20.93

Fig. 3 displays the XRD patterns of fresh ACS-4, $CaSO_4$, CaO and fly ash. Among them, the fly ash was provided by a domestic coal-fired power plant. The major chemical composition of fly ash is shown in Table S2,† and it was characterized by the X-ray fluorescence (XRF) method. The weak diffraction peak of fly ash at $2\theta = 26.5°$ was indexed to quartz (SiO_2). Although fly ash is an essentially vitreous material with numerous amorphous structures, it also contained a small amount of SiO_2 crystalline phases. In addition, peaks of CaO and $CaSO_4$ closely matched the corresponding standard PDF database. Notably, the strong diffraction peaks of ACS-4 at $2\theta = 28.66°$, 34.09°, 47.12°, 50.79°, 54.34°, 56.25°, 62.54° and 64.23° were attributed to $Ca(OH)_2$ (JCPDS PDF No. 36-1248),[35] and the other major diffraction peaks at 2θ = 9.93°,18.02° and 19.76° corresponded well with a $Ca_2Al_3Si_9O_{36}\cdot 8H_2O$ standard (#39-1381).[13] Thus, the diffraction patterns changed appreciably after activation of the original fly ash with CaO/$CaSO_4$. The major phase of the ACS-4 material was calcium aluminate silicate hydrate and calcium hydroxide ($Ca(OH)_2$) with no presence of CaO, $CaSO_4$ and SiO_2. The new component in ACS-4 was considered to be formed in the fly ash/CaO/$CaSO_4$ hydration process during ACS

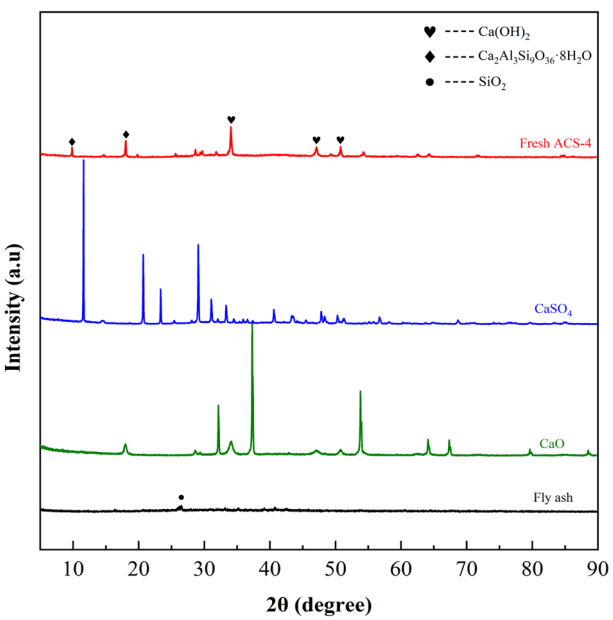

Fig. 3 XRD patterns of the three raw materials and the fresh ACS-4.

preparation. It was further demonstrated that the occurrence of chemical reaction after the mixing of fly ash/CaO/$CaSO_4$ resulted in the formation of calcium aluminate silicate hydrate and calcium hydroxide, dramatically increasing the surface area of the sorbents. Moreover, the XRD patterns of ACS-1, ACS-2, ACS-3 and ACS-5 were similar to that of ACS-4 (shown in Fig. S2†). Hence, the ACS material presents superior desulfurization performance compared with the raw individual components.

Furthermore, the SO_2 adsorption active site in the ACS sorbents was investigated by XRD analysis. As shown in Fig. 4(a), the XRD patterns of fresh and used ACS-4 showed that no new crystal phase was generated in the desulfurization process, suggesting that SO_2 adsorption species were highly dispersed on the surface of the sorbent with no crystallization. After the desulfurization process, peaks at $2\theta = 9.93°$ and 19.76°, attributed to silicate hydrate, almost completely disappeared. Besides, the diffraction peak intensity of calcium hydroxide was weakened.

It was inferred that the silicate hydrate compound and calcium hydroxide were converted to other chemical substances. Furthermore, the pore diameter distributions of ACS-4 before and after desulfurization are shown in Fig. 4(b). As shown in Table 3, the pore volume dropped from 0.176 to 0.094 $cm^3\ g^{-1}$, indicating that SO_2 adsorption species accumulated in the pore structure. Consequently, the sorbents were entirely inactive due to the consumption of adsorption active sites.

The top surface morphologies of fresh ACS-4 and used ACS-4 were observed using SEM. As shown in Fig. 4(c), the porous fiber-like and network structure displayed an ordered microscopic pore structure, which provided a sufficient buffer space for SO_2 adsorption reaction and significantly improved SO_2 diffusion and transformation. Fly ash is typically composed of spherical particles, as shown in Fig. S3.† In addition, Fig. S4† contains the SEM images of fresh ACS-1, ACS-2, ACS-3 and ACS-5, all of which displayed analogous surface morphologies. As shown in Fig. 4(d), ACS-4 was crushed into smaller particles when used in the reactor. Further, during the adsorption of SO_2 molecules, calcium sulfate and calcium sulfite formed, leading to clogging of the channel. It could be observed that the porous fiber-like and network structure of the sorbent was no longer discernible. Furthermore, the thermal stability of the ACS materials was detected with thermogravimetric analysis from 50 °C to 800 °C in an air atmosphere (Fig. S5†). All the samples presented a prominent weight loss peak at around 700 °C, ascribed to the decomposition of the ACS. From 50 to 700 °C, the weight loss of all samples was constant and slow, due to the release of water in the structure. As a result, the ACS remained stable at the practical desulfurization temperature of 150 °C.

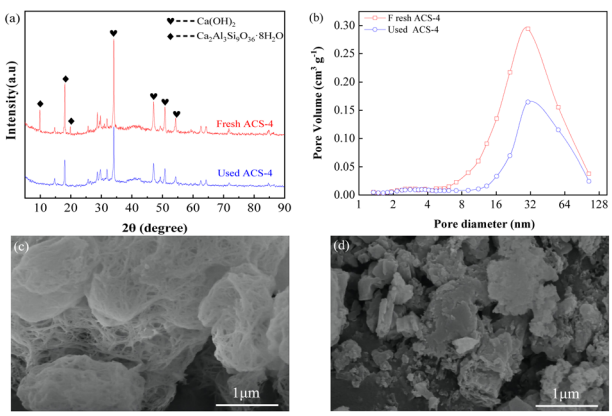

Fig. 4 (a) XRD patterns of fresh ACS-4 and used ACS-4; (b) pore volume distributions of the fresh and used ACS-4. The ACS-4 morphology characterized by SEM: (c) fresh sorbent and (d) used sorbent.

Table 3 Surface area and characteristic pore data of ACS-4 before and after SO_2 adsorption

Samples	S_{BET}, ($m^2\ g^{-1}$)	V_p, ($cm^3\ g^{-1}$)	d_p, (nm)
ACS-4	31.43	0.176	22.34
ACS-4-used	18.13	0.094	20.78

3.3 Desulfurization mechanism

3.3.1 Influence of O_2 on SO_2 adsorption. To investigate the adsorption behavior and species accumulated on the sorbents, *in situ* DRIFTS analysis of SO_2 adsorption on ACS-4 in the absence of O_2 was conducted. Fig. 5(a) shows the variation of the DRIFTS spectra over time with ACS-4 exposed to SO_2/N_2 at 150 °C. Four prominent bands at 1376, 1346, 1130 and 980 cm^{-1} were detected during the SO_2 adsorption process. The bands at 1346 and 1376 cm^{-1} could be assigned to gaseous or adsorbed SO_2,[36] confirming that some SO_2 was adsorbed directly in the form of SO_2 molecules. The relatively weak absorption band observed at 1130 cm^{-1} was assigned to SO_4^{2-} (sulfate) asymmetric stretching.[37] It was speculated that surface adsorbed oxygen species on ACS-4 oxidize SO_2 to SO_4^{2-}. Besides, the vibration absorption peak at 980 cm^{-1}, ascribed to SO_3^{2-}

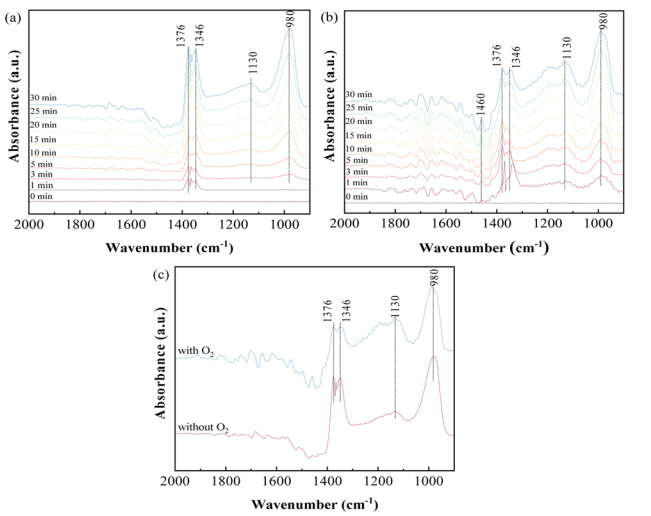

Fig. 5 *In situ* DRIFTS spectra of ACS-4 (a) exposed to 1000 mg m^{-3} SO_2 at 150 °C for various times; (b) exposed to 1000 mg m^{-3} SO_2 and 8% O_2 at 150 °C for various times; (c) comparison spectra at 30 min under the condition of the presence or absence of O_2.

(sulfite),[38] grew increasingly strong over time. It resulted from the adsorbed SO_2 reacting with H_2O/OH^- in ACS-4 to generate a large amount of sulfite species.

To further explore the influence of O_2 on SO_2 removal, the desulfurization reaction was carried out for 30 min in the presence of O_2. As shown in Fig. 5(b), bands at 1460, 1376, 1346, 1130 and 980 cm^{-1} were detected, and the intensity of all peaks increased over time. Notably, the band at 1460 cm^{-1} could be assigned to SO_3 molecules adsorbed on the surface of a metal ion by van der Waals force.[39] Different from SO_2 adsorption in the absence of O_2, the intensity of the absorption band at 1130 cm^{-1} (assigned to SO_4^{2-}) increased more rapidly, suggesting that the presence of O_2 promoted the formation of SO_4^{2-} species. When the sample was treated with SO_2 and O_2, the gaseous or adsorbed SO_2 species could still exist, but the intensity of these bands (1346 and 1376 cm^{-1}) was weaker than the band intensity shown in Fig. 5(a).[40] In addition, the peak intensity at 1130 cm^{-1} increased and that at 980 cm^{-1} decreased simultaneously with O_2 addition. For a clearer comparison of the effects of O_2 on SO_2 removal, the spectra of SO_2 adsorption in the presence and absence of O_2 for 30 minutes are shown separately in Fig. 5(c). The results indicate that SO_3^{2-} derived from $CaSO_3$ was oxidized to sulfate by the oxygen. In the presence of oxygen, the peak areas of SO_3^{2-} and SO_4^{2-} increased faster than in the absence of oxygen with increasing reaction time, indicating that oxygen enhanced the reaction of sulfur dioxide with the calcium-based sorbent. In summary, both physical and chemical adsorption occurred in the desulfurization process with SO_2/O_2 as the feed gas.

3.3.2 Influence of NO on SO_2 adsorption. In consideration of NO as one of the major constituents present under practical conditions, the adsorption behavior of $SO_2/NO/O_2$ as the feed gas on ACS-4 was monitored. Firstly, NO adsorption in the absence and presence of O_2 was investigated. Fig. 6(a) illustrates that NO was adsorbed weakly on the surface of ACS-4 after ACS-4 was purged with NO for 30 min. With 8% O_2 included, evident bands at 1639, 1603, 1386, 1358, 1251 and 1081 cm^{-1} were observed. The bands at 1629 and 1603 cm^{-1} were attributed to gaseous or adsorbed O-bound-NO_2,[41] demonstrating that nitric oxide was oxidized to nitrogen dioxide by oxygen. Since NO is not able to be oxidized into NO_2 by O_2 without catalysts at 150 °C,[42] it was inferred that the presence of OH/HO_2 radicals facilitated NO conversion into NO_2, as reported previously.[34]

Besides, the peak at around 1251 cm^{-1} was attributed to nitrite species,[43] and the peaks at 1386 cm^{-1}, 1358 cm^{-1} and 1081 cm^{-1} were related to the vibration of surface nitrate species.[44,45] Hence, generated NO_2 could be converted to calcium nitrite ($Ca(NO_2)_2$) and calcium nitrate ($Ca(NO_3)_2$) by the following equation:

$$2Ca(OH)_2(s) + 4NO_2(g) \rightarrow Ca(NO_3)_2(s) + Ca(NO_2)_2(s) + 2H_2O(l) \quad (4)$$

Furthermore, $SO_2/NO/O_2$ co-adsorption behavior was studied using *in situ* DRIFTS experiments. As shown in Fig. 7(b), the two bands at 1629 and 1603 cm^{-1}, indexed to gaseous or adsorbed O-bound-NO_2, were obviously weakened. This suggested that generated NO_2 was involved in SO_2 removal as a strong oxidant. The peaks at 1376 and 1346 cm^{-1} could be assigned to adsorbed SO_3 molecules. The intensity of the wide bands at 1151 and 1130 cm^{-1}, ascribed to SO_4^{2-} species, was rapidly enhanced during the experiment. Meanwhile, the peak of SO_4^{2-} became more intense and the peak of SO_3^{2-} was weakened in the presence of NO and O_2. The increase of the SO_4^{2-} peak and decrease of the SO_3^{2-} peak were attributed to the oxidizing effect of NO. Therefore, it was suggested that NO_2 was a more powerful oxidant compared with O_2, so it reacted with the SO_2 efficiently at 150 °C. As a result, the presence of O_2 and NO in the feed gas was found to be beneficial to produce sulfate salts instead of sulfite salts as the final product in the desulfurization reaction.

3.4 FTIR analysis

FTIR spectra of the used sorbent in the absence and the presence of NO are shown in Fig. 7. Compared with ACS-4-U, ACS-4-UN exhibits a weak vibration band at around 1384 cm^{-1}, which was assigned to nitrate species.[45] Additionally, the peak at around 1004 cm^{-1}, ascribed to SO_3^{2-} species,[13] disappeared after NO was involved. This further verified that NO can be adsorbed on the surface of ACS-4 and converted into NO_3^-/NO_2^- species. Meanwhile, the presence of NO enabled SO_2/

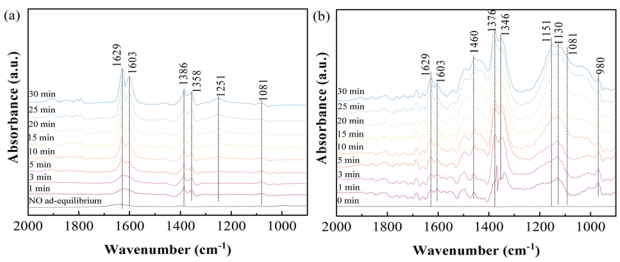

Fig. 6 *In situ* DRIFTS spectra of ACS-4 (a) in a flow of 750 mg m^{-3} NO before and after adding 8% O_2 at 150 °C; (b) in a flow of 1000 mg m^{-3} SO_2, 750 mg m^{-3} NO and 8% O_2 at 150 °C.

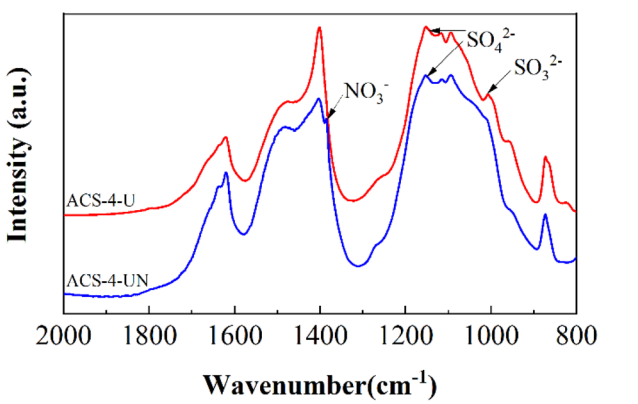

Fig. 7 FTIR spectra of ACS-4-U (without NO) and ACS-4-UN (with 750 mg m^3 NO).

SO_3^{2-} to be oxidized into SO_4^{2-}, enhancing the SO_2 removal efficiency significantly.

3.5 Possible reaction mechanism

Based on *in situ* DRIFTS and FTIR data, it was found that nitrite species (–NO_2), sulfite species (–SO_3), surface-adsorbed SO_2 and SO_3 species and adsorbed-NO_2 species were the main reaction intermediates. In addition, both physical adsorption and chemical reaction were involved in the desulfurization process. Notably, NO played a considerably important role in the SO_2 removal. Adsorbed-NO_2 species, derived from NO, acted as a strong oxidizer for SO_2/SO_3^{2-}. Herein, a possible desulfurization mechanism was proposed, as illustrated in Scheme 1.

In dry flue gas desulfurization (FGD) processes, SO_2 is combined with NO and O_2 to form sulfur trioxide, which is a chemical reaction that can significantly boost the adsorption. Based on the above results, the mechanism of O_2 and NO enhancing SO_2 removal under dry conditions is summarized as follows in reactions (5)–(12).

$$SO_2(g) \rightarrow SO_2(ad) \quad (5)$$

$$SO_2(ad) + Ca(OH)_2(s) \rightarrow CaSO_3(s) + H_2O(l) \quad (6)$$

$$SO_2(ad) + 0.5\ O_2(g) \rightarrow SO_3(ad) \quad (7)$$

$$NO(g) \rightarrow NO(ad) \quad (8)$$

$$NO(ad) + 0.5\ O_2(g) \rightarrow NO_2(ad) \quad (9)$$

$$NO_2(ad) + SO_2(ad) \rightarrow SO_3(ad) + NO(g) \quad (10)$$

$$SO_3(ad) + Ca(OH)_2(s) \rightarrow CaSO_4(s) + H_2O(l) \quad (11)$$

$$3NO_2(ad) + Ca(OH)_2(s) \rightarrow Ca(NO_3)_2(s) + NO(g) + H_2O(l) \quad (12)$$

where (g) and (ad) denote the gaseous and adsorbed states of SO_2, NO, NO_2, and SO_3, respectively.

In accordance with the above chemical equations, O_2 plays an important role in the formation of SO_3. Compared with SO_2, SO_3 can more easily be adsorbed on the surface of the ACS since the sorbent is a material with strong basicity. Moreover, the presence of NO leads to the formation of NO_2, which promotes the oxidation of SO_2 into SO_3. Finally, the adsorption active sites are mainly occupied by SO_4^{2-} species, resulting in deactivation of the ACS.

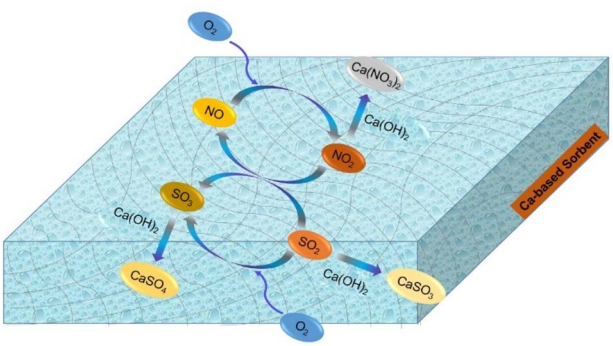

Scheme 1 Desulfurization reaction routes enhanced by the presence of NO and O_2.

4. Conclusions

Flue gas desulfurization (FGD) processes are well-established and prominent technologies for the reduction of SO_2 in post-combustion stack gases emitted from coal-fired processes. In this work, a simple, convenient and green synthesis method was applied to prepare sorbents with high adsorption capabilities in dry FGD processes. Herein, the conclusions drawn are as follows.

Firstly, the high-value utilization of fly ash and gypsum was achieved. Based on our experimental results, the optimum proportion of ACS material for SO_2 removal was coal fly ash/$CaO/CaSO_4 = 1:2:1$. It was found that the capture of SO_2 by the ACS with a specific surface area of 31.5 $m^2\ g^{-1}$ was much higher than that of its raw materials with an adsorption capacity of 44.26 mg g^{-1}, superior to the majority of calcium-based sorbents reported previously. This can be attributed to its relatively large specific surface area, abundant mesopore structure and uniform distribution of pore size. Besides, the newly formed crystalline phase (calcium aluminate silicate hydrate) after the mixing of fly ash, gypsum and CaO acts as active adsorption sites for SO_2, enhancing desulfurization efficiency dramatically.

Therefore, ACS-4 is a valuable and high-performing substitute for conventional sorbents for SO_2 capture. Notably, the impact of O_2 and NO in the desulfurization process was elucidated, which is instructive for the adjustment and improvement of actual working conditions.

Conflicts of interest

There are no conflicts to declare.

Notes and references

1 H. Zhang, J. Niu, Y. Guo and F. Cheng, *J. Cleaner Prod.*, 2021, **280**, 124375.
2 R. Chen, T. Zhang, Y. Guo, J. Wang, J. Wei and Q. Yu, *Chem. Eng. J.*, 2021, **420**, 127588.
3 C. Banerjee, S. Agarwal, P. S. Dash and A. Roy, *Therm. Sci. Eng. Prog.*, 2021, **25**, 101025.
4 Y. Mathieu, L. Tzanis, M. Soulard, J. Patarin, M. Vierling and M. Molière, *Fuel Process. Technol.*, 2013, **114**, 81–100.
5 H. Zhang and A. J. Khan Chowdhury, *Nat., Environ. Pollut. Technol.*, 2019, **18**, 1621–1625.
6 R. del Valle-Zermeño, J. Formosa and J. M. Chimenos, *Rev. Chem. Eng.*, 2015, **31**, 303–327.
7 K. T. Lee, A. M. Mohtar, N. F. Zainudin, S. Bhatia and A. R. Mohamed, *Fuel*, 2005, **84**, 143–151.
8 H. Tamon and M. Okazaki, *Carbon*, 1996, **34**, 741–746.
9 L. Yang, X. Jiang, W. Jiang, P. Wang and Y. Jin, *Energy Fuels*, 2017, **31**, 4556–4564.

10 W. Liao, X. Meng, L. Yao, W. Jiang and L. Yang, *ACS omega*, 2021, **6**, 30949–30959.
11 L. Juan, F. Yu, H. Lihua, T. Deliang, C. Haiyan, N. Belzile and C. Yuwei, *J. Hazard. Mater.*, 2020, **389**, 121914.
12 T. Ishizuka, T. Yamamoto and T. Murayama, *Energy Fuels*, 2001, **15**, 438–443.
13 K. T. Lee, A. R. Mohamed, S. Bhatia and K. H. Chu, *Chem. Eng. J.*, 2005, **114**, 171–177.
14 H. Tsuchiai, H. Nakamura, *et al*, *Ind. Eng. Chem. Res.*, 1996, **35**, 851–855.
15 N. A. Khan, Z. Hasan and S. H. Jhung, *Chem.–Eur. J.*, 2014, **20**, 376–380.
16 P. Maina, *Proceedings of the Sustainable Research and Innovation Conference*, 2022, vol. 35, pp. 140–149.
17 T. Ishizuka, H. Tsuchiai, T. Murayama, T. Tanaka and H. Hattori, *Ind. Eng. Chem. Res.*, 2000, **39**, 1390–1396.
18 G. Jun, Y. Sam and C. Nag, *Appl. Sci.*, 2018, **8**, 1116.
19 N. Karatepe, A. Ersoy-Mericboyu and S. Küçükbayrak, *Environ. Technol.*, 1999, **20**, 377–385.
20 N. F. Zainudin, K. T. Lee, A. H. Kamaruddin, S. Bhatia and A. R. Mohamed, *Sep. Purif. Technol.*, 2005, **45**, 50–60.
21 Y. Wang, X. Han, M. Chen, S. Cui, X. Ma and L. Hao, *Materials*, 2020, **14**, 68.
22 N. N. Abd Malek and R. Laiman, *Sci. Lett.*, 2018, **12**, 63–76.
23 V. H. Dodson, *Concrete admixtures*, Springer, 1990, pp. 159–201.
24 I. Dahlan, K. T. Lee, A. H. Kamaruddin and A. R. Mohamed, *Environ. Sci. Technol.*, 2008, **42**, 1499–1504.
25 W. Jozewicz and G. T. Rochelle, *Environ. Prog.*, 1986, **5**, 219–224.
26 P. Davini, *Fuel*, 1996, **75**, 713–716.
27 J. Fernandez, J. Renedo, A. Garea, J. Viguri and J. Irabien, *Powder Technol.*, 1997, **94**, 133–139.
28 H. Son, S. M. Park, J. H. Seo and H. K. Lee, *Materials*, 2019, **12**, 1673.
29 M. Cui, F. Niu, N. Wang, J. Zhou, J. Wang and J. Li, *Fuel*, 2020, **277**, 118051.
30 B. Yang, S. Ma, R. Cui, S. Sun, J. Wang and S. Li, *Chem. Eng. J.*, 2019, **359**, 233–243.
31 F. Wang, Y. Zhang and Z. Mao, *New J. Chem.*, 2020, **44**, 11879–11886.
32 D. Barpaga and M. D. LeVan, *Microporous Mesoporous Mater.*, 2016, **221**, 197–203.
33 Z. Ling, P. Wan, C. Yu, N. Xiao, J. Yang, Y. Long and J. Qiu, *Chem. Eng. J.*, 2015, **259**, 894–899.
34 W. Kurdowski, *Cement and concrete chemistry*, Springer Science & Business, 2014.
35 Z. Mirghiasi, F. Bakhtiari, E. Darezereshki and E. Esmaeilzadeh, *J. Ind. Eng. Chem.*, 2014, **20**, 113–117.
36 Y. Yu, J. Wang, J. Chen, X. Meng, Y. Chen and C. He, *Ind. Eng. Chem. Res.*, 2014, **53**, 16229–16234.
37 M. Yan, F. Chen, J. Zhang and M. Anpo, *J. Phys. Chem. B*, 2005, **109**, 8673–8678.
38 T. Ishizuka, H. Kabashima, T. Yamaguchi, K. Tanabe and H. Hattori, *Environ. Sci. Technol.*, 2000, **34**, 2799–2803.
39 L. Wei, S. Cui, H. Guo, X. Ma and L. Zhang, *J. Mol. Catal. A: Chem.*, 2016, **421**, 102–108.
40 X. Dong, L. Huang, C. Hu, H. Zeng, Z. Lin, X. Wang, K. M. Ok and G. Zou, *Angew. Chem.*, 2019, **131**, 6598–6604.
41 X. Wu, Q. Liang, D. Weng and Z. Lu, *Catal. Commun.*, 2007, **8**, 2110–2114.
42 N. Guillén-Hurtado, A. Bueno-López and A. García-García, *Appl. Catal., A*, 2012, **437**, 166–172.
43 J.-Y. Ye, J.-L. Lin, Z.-Y. Zhou, Y.-H. Hong, T. Sheng, M. Rauf and S.-G. Sun, *J. Electroanal. Chem.*, 2018, **819**, 495–501.
44 X. Feng, S. Zhang, R. Liu, J. Ma, X. Xu, J. Xu, X. Fang and X. Wang, *Phys. Chem. Chem. Phys.*, 2022, **24**, 3250–3258.
45 X. Duan, D. Yuan, X. Wang and H. Xu, *J. Sol-Gel Sci. Technol.*, 2005, **35**, 221–224.